Final Report

A Lagrangian approach to capture the unsteady aerodynamics of insect-like flapping flight

AFOSR/AOARD Reference Number : AOARD-09-4100
AFOSR/AOARD Program Manager: Dr. John Seo, Lt. Col., USAF
Period of Performance: August 2008-July 2010

PI: Dr. Sunetra Sarkar
IIT Madras, Chennai, India.
Email: sunetra.sarkar@gmail.com

September 9, 2010

Report Documentation Page

Form Approved
OMB No. 0704-0188

1. REPORT DATE	2. REPORT TYPE	3. DATES COVERED
16 SEP 2010	**FInal**	**01-08-2008 to 01-07-2010**

4. TITLE AND SUBTITLE
A Lagrangian Approach to Capture the Unsteady Aerodynamics of Insect-Like Flapping Flight

5a. CONTRACT NUMBER
FA23860914100

5b. GRANT NUMBER

5c. PROGRAM ELEMENT NUMBER

6. AUTHOR(S)
Sunetra Sarkar

5d. PROJECT NUMBER

5e. TASK NUMBER

5f. WORK UNIT NUMBER

7. PERFORMING ORGANIZATION NAME(S) AND ADDRESS(ES)
Indian Institute of Technology Madras,Department of Aerospace Engineering,Chennai 600036,India,IN,600036

8. PERFORMING ORGANIZATION REPORT NUMBER
N/A

9. SPONSORING/MONITORING AGENCY NAME(S) AND ADDRESS(ES)
AOARD, UNIT 45002, APO, AP, 96337-5002

10. SPONSOR/MONITOR'S ACRONYM(S)
AOARD

11. SPONSOR/MONITOR'S REPORT NUMBER(S)
AOARD-094100

12. DISTRIBUTION/AVAILABILITY STATEMENT
Approved for public release; distribution unlimited

13. SUPPLEMENTARY NOTES

14. ABSTRACT

A Lagrangian viscous vortex technique is used in the present study to simulate the unsteady flow field of flapping flight. The method is grid free and computations are done only at the regions of non-zero vorticity. As a result this method is quite suitable for simulating the unsteady vertical flow-field past flapping wings and airfoils; it provides an accurate and fast flow-visualization. The main strength of this tool is its grid free nature; as the resolution of the grid is a crucial parameter in resolving the unsteady flow-field accurately. It is also relatively easy to implement a grid-free particle based technique for a moving boundaries or complex geometries. In this algorithm, field property vorticity is carried by discrete particles which convects with the Biot-Savart velocity and diffuses with random walk.

15. SUBJECT TERMS
Micro Air Vehicles (MAVs), Unsteady Flow, Computational Aerodynamics, Computational Fluid Dynamics (CFD)

16. SECURITY CLASSIFICATION OF:			17. LIMITATION OF ABSTRACT	18. NUMBER OF PAGES	19a. NAME OF RESPONSIBLE PERSON
a. REPORT	b. ABSTRACT	c. THIS PAGE			
unclassified	**unclassified**	**unclassified**	**Same as Report (SAR)**	**18**	

1 Objectives

Experimental results performed on scaled robo-insects give us an idea of the resulting flow-field [1]. The evolution of the vortical flow-field and the resulting aerodynamic load time histories are functions of various geometric and kinematic parameters of the system. An extensive investigation of the parametric space using a grid based Eulerian solver requires enormous time and storage, as the method needs intricate grids to resolve the vortex structures and the boundary layers. They also suffer from numerical diffusion. To bypass these issues, we propose to use a Lagrangian flow solver: it solves the incompressible Navier-Stokes equation in terms of vorticity. The computation is limited to only non-zero vorticity region, which increases computational efficiency. It is also free from grid based numerical diffusion and adapts to complex geometries well.

The broad objective in the first part of the research undertaken is to use a Lagrangian particle based tool and validate its performance using earlier experimental results for fundamental flapping kinematics like pitch and plunge. The specific aim was to find a systematic relationship between these two fundamental kinematics at different parametric regimes. Experimental results for plunge-equivalent pitching cases have been discussed in [2]. In this reference comparison between experimental data and grid-based CFD results show poor agreement for pure pitching cases. The Lagrangian solver would be used to simulate these cases and the results will be compared with that presented in [2]. Results for comparison would be in terms of vorticity flow-fields stream-wise velocity profiles. Another discrepancy that the study [2] reports is, in the experiments the heave-equivalent pure pitching shows vortex street deflection which was not present in its equivalent heaving case. Thus the study addresses a fundamental question, if a heave-equivalent pitch case [3] in indeed equivalent to its heave counterpart, or nonlinear effects are significantly high not to make it so. Based on our Lagrangian solver results, these issue would also be addressed. This study would also consider different deflection modes as a function of the starting conditions.

In the second part of the research undertaken, the heave and pitch motion would be combined together. Many invertebrates' hovering flight relies on this mechanism as a translation in the stroke plane along with wing rotation. The kinematics presents the following important parameters: reduced frequency, phase relation, stroke amplitude, angle of rotation. Varying these parameters gives us the important insight on the flow-field evolution and aerodynamic load generation. This work will look at understanding the unsteady load generating mechanism for hover. One of the main mechanism used by insects to generate large aerodynamic loads is delayed stall. For a wing translating at a large angle of attack, a leading edge vortex is formed at

each half-stroke which remains attached to the body till the end of the half-stroke generating large suction and lift. At the end of a half-stroke, the wing rotates and moves into the vortical region created in its previous half-stroke, sometimes referred to as 'wake capture' [1]. The mechanism of wing acceleration and wake capture were instrumental in increasing the lift force [4] in previous studies on model wing [5] and 3D computations. However, the 3D mechanism is different as there are spanwise flows to stabilize the vortex, though the whole behavior is *Re* dependent [6]. The 2D behavior is expected to be different. For MAV wing which operate at different Reynolds number ranges than the natural species, there is a need to revisit the exercises to resolve its unsteady flow-field. The *Re* range of our concern is around 1000 and the flow lacks the stabilizing effect of span-wise flow.
It is also of interest to modify the present code and make it more efficient. The present code uses a first order time stepping using Euler's method. We would like to increase the time stepping accuracy by including higher order time integration methods for the convection step. In order to improve the flow-field visualization without sacrificing the accuracy, a vortex merging algorithm and some alternate diffusion schemes will also be explored.

2 Status of effort

In the first part, the Lagrangian tool has successfully captured the experimental results for fundamental flapping kinematics [7, 2]. The role of the starting condition in deciding the wake deflection mode for pure pitch and pure plunge is resolved. The role of mean angle of attack has also been commented upon. The Lagrangian tool has also confirmed the earlier findings about the kinematic equivalence of pitch and plunge for a symmetric airfoil. It shows that the quasi-steady criterion and the Theodorsen's approach give the best kinematic equivalence for pitch with its plunge counterpart. This has been investigated for different stroke amplitudes. Simulation has also been done for long time after the first transients are settled in order to search for a second time stationarity. The observation for the symmetric profile is that the deflection mode switching to an upward pattern irrespective of the starting condition which is quite similar to that of a cambered profile reported earlier [8]. We have published these results in [7, 9]. The Lagrangian tool has also been modified as proposed in the objective. A second order Runge-Kutta time stepping algorithm has been successfully implemented. A vortex merging and annihilation scheme has also been introduced. Both of them together make the modified tool faster. A calculation of the aerodynamic loads verify the accuracy of the modified code as well. A test case of a circular cylinder is validated successfully with this. A sinusoidal hover case is investigated with

the modified code at a moderate Reynolds number around 3000. The flow field is compared for its aerodynamic loads with its low Reynolds number counterpart for which experimental results are available in the literature.

3 Abstract

A Lagrangian viscous vortex technique is used in the present study to simulate the unsteady flow field of flapping flight. The method is grid free and computations are done only at the regions of non-zero vorticity. As a result this method is quite suitable for simulating the unsteady vortical flow-field past flapping wings and airfoils; it provides an accurate and fast flow-visualization. The main strength of this tool is its grid free nature; as the resolution of the grid is a crucial parameter in resolving the unsteady flow-field accurately. It is also relatively easy to implement a grid-free particle based technique for a moving boundaries or complex geometries. In this algorithm, field property vorticity is carried by discrete particles which convects with the Biot-Savart velocity and diffuses with random walk. Heave and pitch kinematics are fundamental to any flapping type MAVs. A set of pure sinusoidal plunging and its kinematically equivalent pitching using the same reduced frequency are investigated. The focus lies in investigating the advantage of the Lagrangian method over grid based CFD solvers in capturing the flow field. Experimental observations have been taken as benchmark for different cases considered. Effect of mean angle, starting conditions, nondimensional stroke amplitudes are considered. One of the main questions considered here is if there exists a kinematic equivalence between sinusoidal pitch and plunge.
In the subsequent part, sinusoidal hovering of a symmetric airfoil at moderate Reynolds number is studied. In the present study, simulation of flow over a flapping airfoil during sinusoidal hover is studied. Calculating the aerodynamic loads is our primary concern. The flow field is simulated with a modified version of the earlier used Lagrangian tool. A higher order tome stepping approach is implemented, also a vortex annihilation and merging scheme is used now.The unsteady flow-field is resolved for a moderate Reynolds number around 3000 which is applicable to various man-made flapping devices like Micro Aerial Vehicles (MAVs). This flapping behavior is also compared with its low Reynolds number counterpart in order to verify any changes in aerodynamic loads. This is done with a grid-based solver as the Lagrangian solver shows somewhat poor convergence behavior at low Reynolds number regime.

4 Personnel

4.1 Personnel supported through contract

Post	Personnel Name	Period of Performance
Project Associate	Anil Agarwal	January 2010-May2010
Project Associate	Vishwanath Singasani	August 2008-April 2009.

4.2 Personnel participated in research but not supported through contract

Degree/Post	Personnel Name	Period of Participation
Masters Student	Anush Krishnan	August 2009-July 2010
Masters Student	Lalit Chandravanshi	August 2009-July 2010

5 Publications

- Sunetra Sarkar, Vishwanath Singasani, Comparison of Fundamental Flapping Kinematics of an Airfoil, AIAA-2009-3815, 39th AIAA Fluid Dynamics Conference, San Antonio, USA, June 2009.
- Sunetra Sarkar, Comparing pure-pitch and pure-plunge kinematics for a symmetric airfoil, accepted, AIAA Journal, 2010.
- Lalit Chandravanshi, Sandip Chajjed, Sunetra Sarkar, Study of wake pattern behind an oscillating airfoil, accepted for publication in the Proceedings of the 37^{th} International and 4^{th} National Conference on Fluid Mechanics and Fluid Power, Chennai, India, December 2010.
- Anush Krishanan, Sunetra Sarkar, Sandip Chajjed, Simulation of flow over a flapping airfoil using a random vortex method, to be submitted, 2010.

6 Interactions

6.1 (a) Participation/presentation at meetings, conference, seminars

- Proceedings of the Indo-US Workshop on Micro Air Vehicles, Bangalore, India, November 2008.
- 39th AIAA Fluid Dynamics Conference, San Antonio, USA, June 2009

6.2 (b) Knowledge resulting form research in technology applications

Not applicable.

7 Inventions

7.1 Discoveries, inventions, patents

None

7.2 Report of invention and subcontracts

DD Form 882 attached.

8 Honors/Awards

None

9 Archival Documentation

For the first part of the research effort we would like to refer to our manuscript accepted for publication in AIAA journal. We are attaching a copy of the accepted version of the manuscript. A technical description of the latter part of the study is given below:

9.1 Simulation of Flow over a Flapping Airfoil using a Random Vortex Method

9.1.1 The modified Lagrangian solver

This is a grid-free technique and the flow-field is described by a number of discrete particles carrying field property vorticity. The incompressible Navier-Stokes equation is solved in terms of the vorticity. Velocity field is computed from the Bio-Savart law, obtained from the vector Poisson equation of vorticity-stream function. Various diffusion models can be used in order to simulate viscous diffusion. In our work, a random walk model is used [10]. In some of our earlier works, this Lagrangian method was used to simulate the unsteady flow-field related to dynamic stall and heaving-propulsion [11, 12].

The two-dimensional incompressible Navier-Stokes equation in the vorticity-transport form is shown as [13]:

$$\frac{D\Omega}{Dt} = \nu \nabla^2 \Omega. \tag{1}$$

where ν is the kinematic viscosity, vorticity $\vec{\Omega} = \nabla \times \vec{V}$ with $\vec{V}$ the velocity field. The vorticity and the velocity field is given by a vector Poisson equation [13, 14]

$$\nabla^2 \vec{V} = -\nabla \times \vec{\Omega}. \tag{2}$$

The solution to this vector Poisson equation uniquely defines the velocity-vorticity relationship, known as the Biot-Savart law [13, 14, 15] as shown below.

$$\vec{V}(\vec{r}, t) = -\frac{1}{2\pi}\left[\int_{\mathrm{R}} \frac{\vec{\Omega} \times (\vec{r}_0 - \vec{r})}{|\vec{r}_0 - \vec{r}|^2} d\mathrm{R} + 2\int_{\mathrm{S}} \frac{\vec{\Omega}_b \times (\vec{r}_0 - \vec{x})}{|\vec{r}_0 - \vec{x}|^2} d\mathrm{S} + \vec{V}_\infty\right], \tag{3}$$

where $\vec{\Omega}_b$ is the rigid body angular velocity of the solid whose boundary is denoted by S, and $\vec{V}_\infty$ its translational velocity. $\vec{r}_0$ is the vector distance from the origin of the reference frame to the vortex particles in the fluid region R, and $\vec{r}$ is the point in the flow-field where the induced velocity due to these vortex particles are to be determined. Note that the velocity field automatically satisfies the far-field velocity boundary condition of the flow. The vorticity field is discretized as a collection of vortex particles, each with an associated circulation strength. The vorticity at any point in the flow domain is given by,

$$\Omega(\vec{r}) = \sum_{j=1}^{N} \Gamma_j f_\delta(\vec{r} - \vec{r}_j). \tag{4}$$

We assume there ate N vortex particles at locations $\vec{r}_j$ with circulations Γ_js respectively; f_δ is a function that defines the vorticity distribution, and therefore the induced velocity distribution of the blob. In the present work, Chorin blob model is used as the basic vortex particles. The induced radial velocity field due to a Chorin blob is given by,

$$\begin{aligned} V(r) &= \frac{\Gamma}{2\pi\sigma}, \quad \text{when} \quad r \leq \sigma \\ &= \frac{\Gamma}{2\pi r}, \quad \text{when} \quad r > \sigma \end{aligned} \tag{5}$$

The overall velocity field consists of a rotational and an irrotational part. The rotational component of the flow velocity is obtained from the velocity induced by the vortex blobs. The contribution from the solid body is computed

by approximating the solid area using square elements and summing over the contributions from each of them. The irrotational component is obtained by solving for potential flow using the appropriate boundary conditions- the non-penetration of flow at the solid surface in this case. This is done by using a panel method type formulation. According to this, a vortex sheet is assumed to be attached to the solid region boundary. The boundary is subdivided into line segments with a linear vortex sheet strength distribution over each such segments or panels. The induced velocity velocity field in complex notation due to a panel with endpoints z_1 and z_2 and sheet strength distribution varying from γ_1 to γ_2 is given by,

$$\begin{aligned} V(z) &= u - iv \\ &= \Big[-\frac{i\gamma_1}{2\pi}\Big\{\Big(\frac{z'}{\lambda}-1\Big)\ln\Big(\frac{z'-\lambda}{\lambda}\Big)+1\Big\} + \frac{i\gamma_2}{2\pi}\Big\{\frac{z'}{\lambda}\ln\Big(\frac{z'-\lambda}{\lambda}\Big)+1\Big\}\Big]\mathrm{e}^{i\theta} \end{aligned} \tag{6}$$

where, $z' = (z - z_1)\mathrm{e}^{i\theta}$ and θ is the angle made by $z_1 - z_2$ with the real axis. The velocity distribution over all panels is calculated such that the condition $(V_{\text{irrotational}} + V_{\text{rotational}}).\hat{n} = V_{\text{body}}.\hat{n}$ is satisfied at specific control points along the surface, which we choose as the mid-points of each panel. An additional condition concerning the total circulation over the body also needs to be satisfied []:

$$\int_S \gamma(s)ds = 2A_b\Omega_b(t+\Delta t) - \sum_j \Gamma_j(t) \tag{7}$$

The derived set of equations are solved to obtain the vortex sheet strength distributed along the body surface. This, in general will not ensure a 'no-slip' at the body surface. The 'no-slip' condition $V_{\text{fluid}} = V_{\text{body}}$ required for viscous flows is ensured by releasing the Chorin vortex blobs from the body surface. These blobs are generated at the panel control points with a circulation strength $V_{\text{slip}}ds$ and a core radius of $ds/(2\pi)$. Here, ds is the individual panel length. As per this model, such a blob will induce a core velocity of V_{slip} in the tangential direction which will nullify the existing slip velocity at the body surface.

We use a operator splitting technique proposed by Chorin [10] in which Eq. (1) can be split into convection and diffusion parts that are to be solved sequentially. This is represented as,

$$\partial\Omega/\partial t + \vec{V}.\nabla\Omega = 0, \quad \text{and} \quad \partial\Omega/\partial t = \nu\nabla^2\Omega \tag{8}$$

This method is also known as 'viscous splitting' and its convergence has been discussed by Beale and Majda [16].

The convection part in Eq. (8) shows the invariance of vorticity of the vortex particles as they move with the fluid. The convection velocity of the blobs

are their self-induced velocity as given by the Bio-Savart law. A second order Runge-Kutta time stepping scheme is employed to convect the blobs:

$$\vec{x}_j(t + \Delta t/2) = \vec{x}_j(t) + \vec{V}_j(t)\frac{\Delta t}{2}$$
$$\vec{x}_j(t + \Delta t) = \vec{x}_j(t + \Delta t/2) + \vec{V}_j(t + \Delta t/2)\frac{\Delta t}{2}. \quad (9)$$

Here, the convection displacement of the j^{th} particle is denoted by $\vec{x}_j$.
The solution of the diffusion part in Eq. (8) is given by a Gaussian probability density function [13]. A random walk algorithm [10] is used to approximate diffusion [17, 18]. At the end of the convection step, the vortex blobs are given a diffusion displacement of η_x, η_y, whete η_x and η_y are random variables generated with Gaussian probability distribution with zero mean and standard deviation of $\sqrt{2\nu\Delta t}$. Recently Eldredge [19] and his co-workers have also used a viscous vortex particle method (VVPM) using a deterministic diffusion model to study flapping kinematics of airfoils. In another investigation, A blob annihilation and merging algorithm is also used where blobs of opposite circulation that are closer than a specified distance are replaced with a blob of circulation strength equal to the sum of those of the two blobs, located at their mid-point and having their average blob radius. This reduces the computation time considerably and cleans up the flow-field. The aerodynamic load comparisons showed that it did not introduce significant errors.

9.1.2 Validation: an impulsively started cylinder

The case of an impulsively started uniformly moving cylinder has been studied extensively in the literature and quite a number of excellent benchmark data are available. In particular, Koumousatkos and Leonard [20] have obtained accurate drag coefficient results from high-resolution computations. This case is revisited here to validate the present code. The solid surface of the circular cylinder is subdivided into 400 panels, and a non-dimensional time step of 0.03 has been chosen. Time is non-dimensionalized with respect to the cylinder velocity and the radius. The annihilation distance is chosen to be the average panel length. The results obtained for a Reynolds number of 3000. The initial flow-field and the onset of the Karman vortex structure is shown in Fig. 1 and compared with [21]. The calculated drag coefficient is seen to follow the general trend of the validation data [20]. Due to the stochastic nature of the random vortex method, too much statistical noise is introduced in the high frequency solutions. However, the method gives good engineering results and can be used to determine aerodynamic loads for lower resolution cases. A slightly lower resolution computation is also

carried out for the same Reynolds number with the circular cylinder divided into 300 panels and a non-dimensional time step of 0.24. The computations are carried out till the von Karman flow patterns is visible after the initial transients. The average drag coefficient is computed to be 1.49. The Strouhal number based on the frequency of the vortex shedding is 0.2, quite close to earlier predicted results of 0.21 in the literature [22].

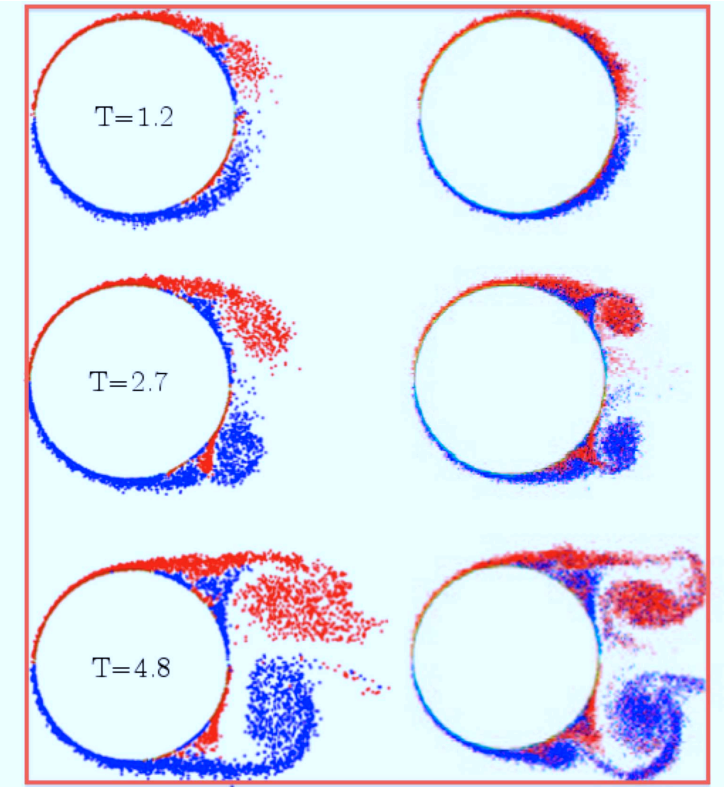

Figure 1: Starting flow-field for impulsively started circular cylinder and validation with earlier work; left column is the present work, right column is from the earlier computations of [21]

9.1.3 Combined Pitch and Plunge in Hover

In the next part of our studies, the Lagrangian code is modified. A blob annihilation and merging algorithm has been used now. This makes the Lagrangian code more efficient and improves the flow visualization. Here, blobs of opposite circulation that are closer than a specified distance are replaced with a blob of circulation strength equal to the sum of those of the two blobs, located at their mid-point and with their average blob radius.

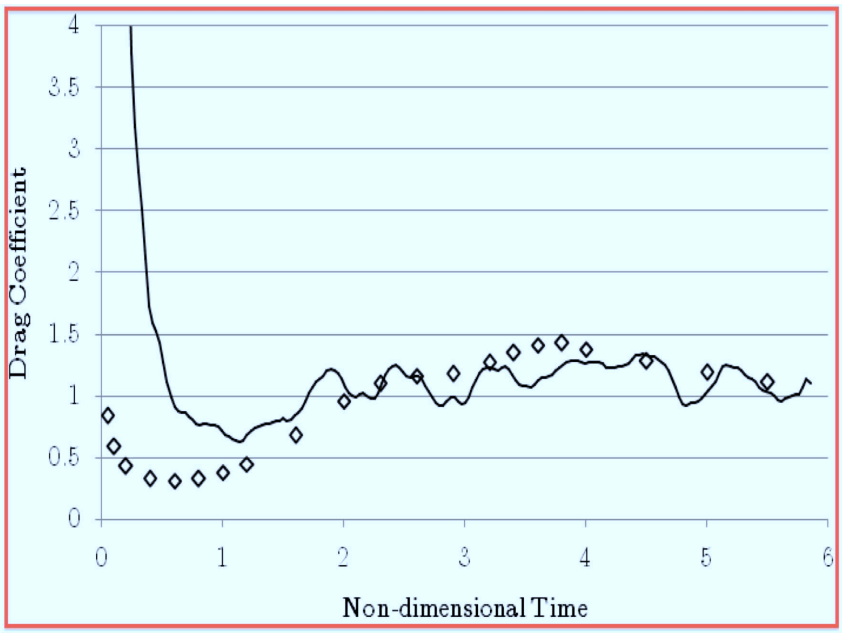

Figure 2: Impulsively started circular cylinder: Validation of the drag coefficient with [20]; solid line represents the present work, diamonds are for the results given in [20]

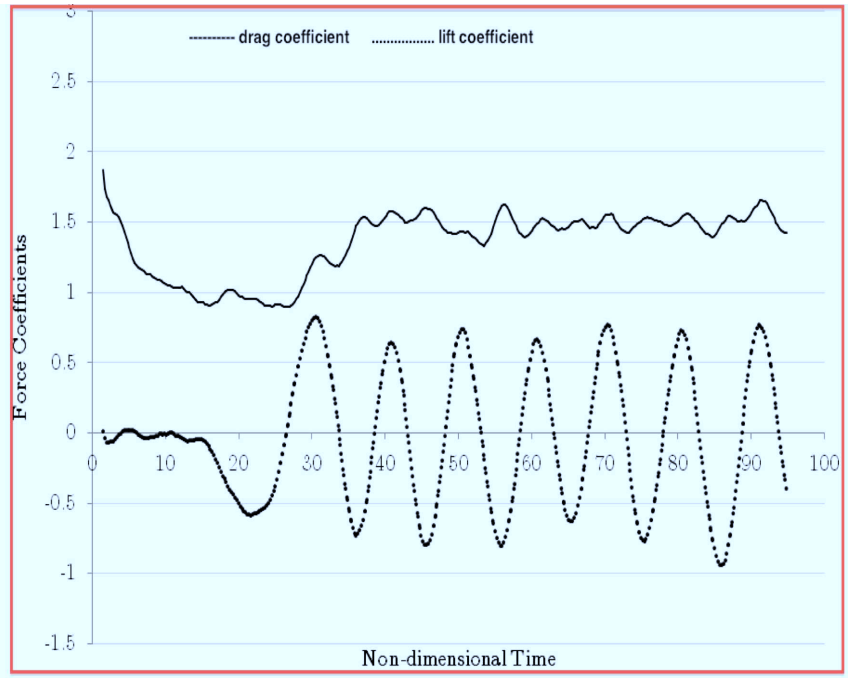

Figure 3: Impulsively started circular cylinder: Load time histories.

This reduces the computation time significantly and cleans up the flow-field; load comparisons showed that it did not introduce significant errors. The forces on the solid body are now calculated from the impulse formula [13]:

$$\frac{\vec{F}}{\rho} = -\frac{d}{dt}\int_D (\vec{y} \times \vec{\Omega}) d\vec{y} + A_b \frac{d\vec{V}_b}{dt} - 2A_b \frac{d}{dt}(\vec{x}_b \times \vec{\Omega}_b) \tag{10}$$

The present section looks at understanding the unsteady load generation mechanism during hover. One of the main load generation mechanism for hovering insect is delayed stall. For a wing translating at a large angle of attack, a leading edge vortex is formed at each half-stroke which remains closely attached to the body till the end of the half-stroke, generating large suction and lift. At the end of the half-stroke, the wing rotates and moves into the vortical region created in its previous half-stroke and experiences increased lift, sometimes referred to as wake capture. The mechanism of wing rotation and wake capture were found to be important contributors to lift in previous studies on model wings [5, 23] and 3-D computations. In 3-D flapping wings, spanwise flows stabilize the leading edge vortex, though the overall behavior is dependent on Re [6]. The 2-D behavior is expected to be different. For MAV wings which operate at different Re ranges than insect species, there is a need to revisit the exercise to resolve its unsteady flow-field. The Re range of our concern is around 3000 and the flow is two dimensional.

In this section, we present results for sinusoidal hover [24]. Once again a symmetric airfoil is chosen. The wing follows a sinusoidal plunging and pitching motion. Specifically the wing sweeps the horizontal plane and pitches about its spanwise axis with a frequency f:

$$\begin{aligned} x(t) &= \frac{A_0}{2}\cos(2\pi f t) \\ \alpha(t) &= \alpha_0 + \beta \sin(2\pi f t + \phi) \end{aligned} \tag{11}$$

where $x(t)$ is the position of the centre of the airfoil, and $\alpha(t)$ is the angle of attack with respect to the x-axis. The parameters α_0 , β, f and ϕ are fixed at $\pi/2$, $\pi/4$, 0.25 Hz and $\pi/4$. A_0/c is 4.0 and the Reynolds number is chosen to be 1000π, non-dimensionalised with respect to the maximum translational velocity of the centre of the airfoil, $\pi f A_0$. The Reynolds number chosen is much higher than that used in [24] as could be the case with MAVs. The convergence and accuracy of the random vortex method is also expected to be much better at higher Re than its very low counterparts as the magnitude of error in a random vortex method is of $O(Re^{-1/2})$ [10]. Larger insects or MAVs may operate at this specified range. Fig.4 shows the evolution of the vorticity field during the first cycle of flapping with the specified kinematics. Red

vortex particles show clock-wise circulation and blue denotes anti-clockwise circulation. Since a stochastic method is being used for simulation, the flow obtained from different runs might have minor variations. But the major features of the flow always appear.

Due to the high angle of attack, a leading edge vortex develops that causes an initial increase in lift till about quarter-stroke after which the lift begins to drop when the vortex is shed. One trailing edge vortex is shed in the beginning of the stroke and by half-stroke, two more are shed. At the end of the half-stroke, the airfoil changes direction and moves into pair of counter rotating vortices shed earlier. The airfoil then moves through them, releasing two vortex dipoles from the leading and trailing edges formed due to pairing between the vortices shed in the downstroke and the newly shed vortices in the upstroke. The lift then sees further increase due to the formation of a new leading edge vortex, and decreases again when it is shed. At the end of the stroke, the airfoil appears to move into another pair of counter rotating vortices, but this time the trailing edge vortex is weaker. The variation of lift coefficient is plotted in Fig. 5 during the first cycle. The decrease in lift observed when the counter rotating wake vortex pair is fully destroyed by the airfoil moving through it leads us to believe that wake capture plays an important role in lift generation in flapping airfoils. But an increase in lift is observed even before the end of the half-stroke which could imply that the rotational forces generated by the body rotation are responsible for the increase in lift, as the airfoil has not moved into the wake yet. Moreover, the decrease in lift also coincides with the point of minimum angular velocity. This has previously been dealt with Sun and Tang [4], whose computations led them to assert that rotational forces were the cause as opposed to the wake capture explanation inferred from the experiments of Dickinson et al [1]. The more important mechanism for lift generation is the formation of the leading edge vortex when the airfoil is near the mean position of plunging. The higher translational velocity as well as the delayed stall effect produces greater lift than the aforementioned causes and give rise to the higher peak in the lift coefficient curve. It is also observed that more vortices shed and interact in comparison to lower Re case. In particular, dipoles are formed from both the leading and trailing edge vortices in contrast to a single dipole formed from the trailing edge alone at lower Re [25, 19].

After the initial transients it was observed that the lift generated during the upstroke was more than that during the downstroke. Load time histories are plotted in Fig. 6. The visualizations during the third and fourth cycle (not shown here) reveal that the leading edge vortex is not formed properly during the downstroke. Hence the asymmetry between the half-strokes. Asymmetry in the lift curve between the half-strokes has also been observed at lower Re for similar kinematics [24].

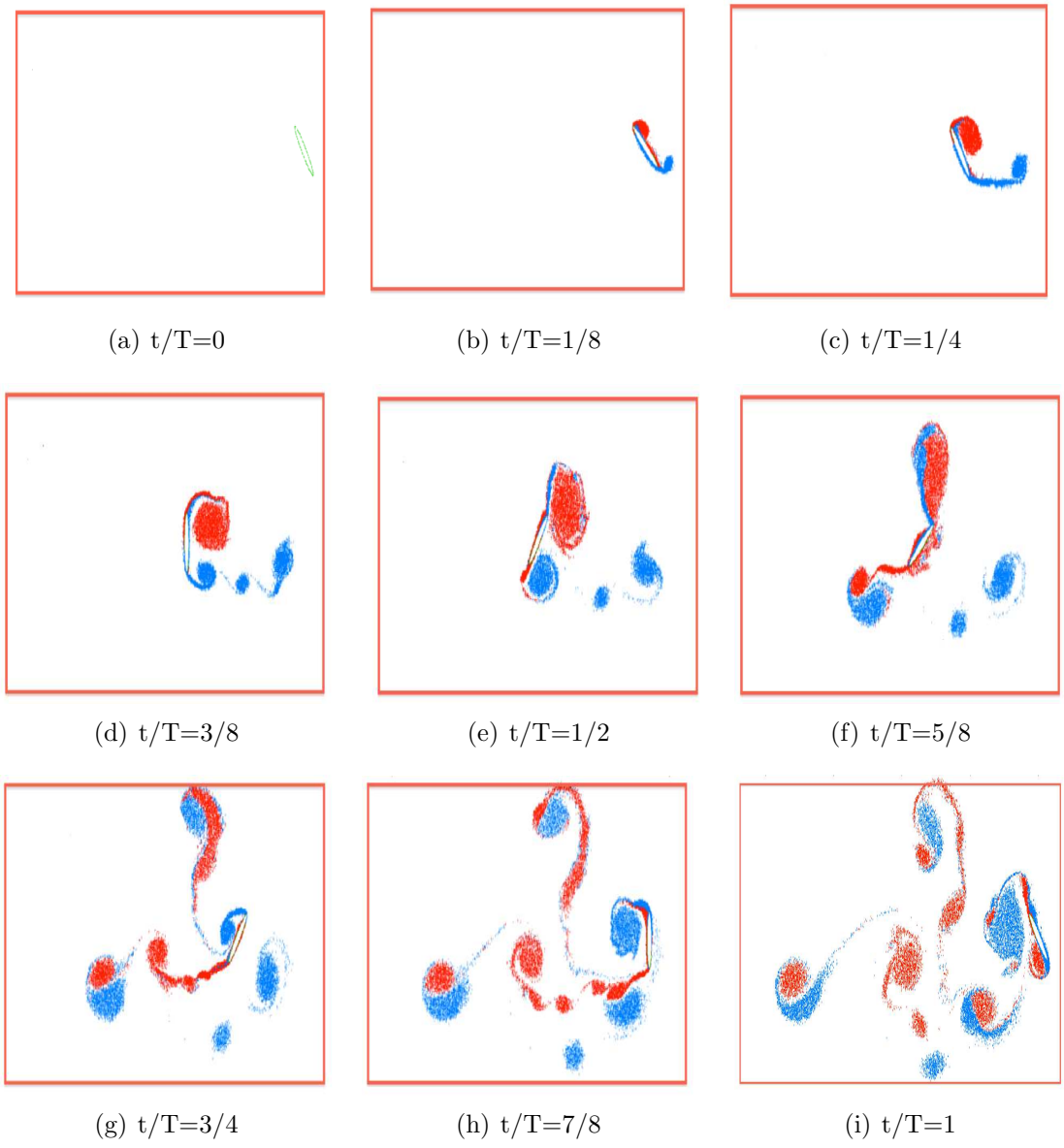

(a) t/T=0 (b) t/T=1/8 (c) t/T=1/4

(d) t/T=3/8 (e) t/T=1/2 (f) t/T=5/8

(g) t/T=3/4 (h) t/T=7/8 (i) t/T=1

Figure 4: Evolution of the vorticity field during the first cycle of the flapping airfoil with the specified kinematics and the flow parameters. Red vortex particles denote clockwise circulation and blue vortex particles denote anti-clockwise circulation. Time during the cycle is mentioned as a fraction of the time period.

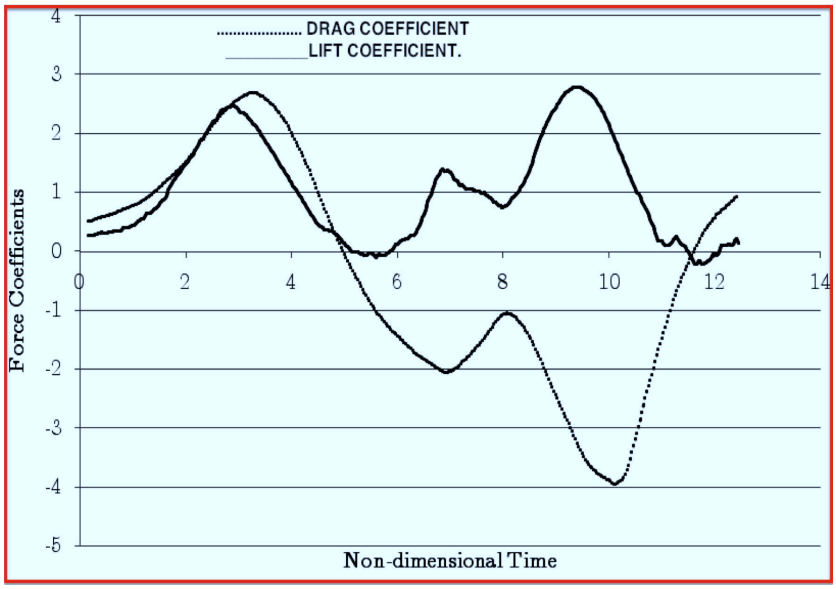

Figure 5: Variation of force coefficients over one cycle for a sinusoidally flapping wing with specified kinematics and flow parameters. The airfoil surface was divided into 400 panels and the non-dimensional time step was 0.01π.

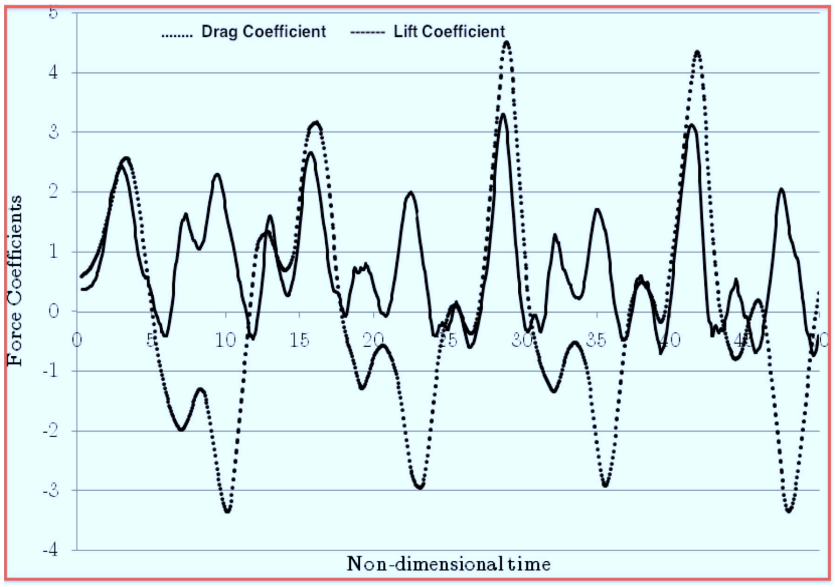

Figure 6: Variation of force coefficients over four cycles for a sinusoidally flapping wing with specified kinematics and flow parameters.

10 Software/Hardware

Not applicable

References

[1] Dickinson, M. H., Lehmann, F. O., and Sane, S. P., "Wing rotation and the aerodynamic basis of insect flight," *Science*, Vol. 284, 1999, pp. 1954–1960.

[2] McGowan, G. Z., Gopalarathnam, A., Ol, M. V., Edwards, J. R., and Fredberg, D., "Computation vs. experiment for high-frequency low-Reynolds number airfoil pitch and plunge," *AIAA* paper *2008-653*, Jan. 2008.

[3] McCroskey, W. J., "The phenomenon of dynamic stall," *NASA-TM-81264*, 1981.

[4] Sun, M. and Tang, J., "Unsteady aerodynamic force generation by a model fruit fly wing in flapping motion," *The Journal of Experimental Biology*, Vol. 205, 2002, pp. 1507–1518.

[5] Sane, S. P. and Dickinson, M. H., "The aerodynamic effects of wing rotation and a revised quasi-steady model of flapping flight," *The Journal of Experimental Biology*, Vol. 205, 2002, pp. 1087–1096.

[6] Birch, M. J., Dickson, W. B., and Dickinson, M. H., "Force production and flow structure of the leading edge vortex on flapping wings at high and low Reynolds numbers," *The Journal of Experimental Biology*, Vol. 207, 2004, pp. 1063–1072.

[7] Sarkar, S., "Comparing pure pitch and pure plunge kinematics for a symmetric airfoil," *AIAA Journal, accepted*, 2010.

[8] Alam, M., Suzen, Y. B., and Ol, M. V., "Numerical simulation of pitching airfoil flowfields for MAV applications," *AIAA* paper*2009-4029*, June, 2009.

[9] Sarkar, S. and Singasani, V., "Comparison of fundamental flapping kinematics of an airfoil," *AIAA* paper *2009-3815*, Jan., 2009.

[10] Chorin, A., "Numerical study of slightly viscous flow," *Journal of Fluid Mechanics*, Vol. 57(4), 1973, pp. 785–796.

[11] Sarkar, S. and Venkatraman, K., "Influence of pitching angle of incidence on the dynamic stall behavior of a symmetric airfoil," *European Journal of Mechanics B/Fluids*, Vol. 27, 2008, pp. 219–238.

[12] Sarkar, S. and Venkatraman, K., "Numerical simulation of incompressible viscous flow past a heaving airfoil," *International Journal of Numerical Methods in Fluids*, Vol. 51, 2006, pp. 1–29.

[13] Batchelor, G., *An introduction to fluid dynamics*, Cambridge University Press, New Delhi, 1967.

[14] Wu, J. and Thompson, J., "Numerical solutions of time-dependent incompressible Navier-Stokes equations using an integro-differential formulation," *Computers and Fluids*, Vol. 1, 1973, pp. 197–215.

[15] Lin, H., Vezza, M., and McD. Galbraith, R., "Discrte vortex method for simulating unsteady flow around pitching aerofoils," *AIAA Journal*, Vol. 35(3), 1997, pp. 494–499.

[16] Beale, J. T. and Majda, A., "Rates of convergence for viscous splitting of the Navier-Stokes equations," *Mathematics of Computation*, Vol. 37, pp. 243–259.

[17] Fogelson, A. and Dillon, R., "Optimal smoothing in function-transport particle methods for diffusion problems," *Journal of Computational Physics*, Vol. 109, 1993, pp. 155–163.

[18] Fishelov, D., "A new vortex scheme for viscous flows," *Journal of Computational Physics*, Vol. 86, 1990, pp. 211–224.

[19] Eldredge, J. D., Wang, C., and Ol, M. V., "A Computational study of a canonical pitch-up, pitch-down wing maneuver," *AIAA* paper *2009-3687*, June, 2009.

[20] Koumoutsakos, P. and Leonard, A., "High-resolution simulations of the flow around an impulsively started cylinder using vortex methods," *Journal of Fluid Mechanics*, Vol. 296, 1995, pp. 1–38.

[21] Ramachandran, P., "Development and Study of a High-Resolution Two-Dimensional Random Vortex Method." *PhD Thesis, Aerospace Engineering, Indian Institute of Technology Madras. Chennai*, 2004.

[22] Fey, U., Koenig, M., and Eckelmann, H., "A new StrouhalReynolds-number relationship for the circular cylinder in the range $47 < Re < 2x10^5$," *Physics of Fluids*, 1998, pp. 1547–1549.

[23] Birch, M. J. and Dickinson, M. H., "The influence of wing-wake interactions on the production of aerodynamic forces in flapping flight," *The Journal of Experimental Biology*, Vol. 206, 2003, pp. 2257–2272.

[24] Wang, Z. J., Birch, M. J., and Dickinson, M. H., "Unsteady forces and flows in low Reynolds number hovering flight: two dimensional computations vs. robotic wing experiments," *The Journal of Experimental Biology*, Vol. 207, 2004, pp. 449–460.

[25] Wang, Z. J., "Two dimensional mechanism for insect hovering," *Physical Review Letters*, Vol. 85, 2000, pp. 2216–2219.